Available online at www.sciencedirect.com
SCIENCE DIRECT®
Journal of Catalysis 223 (2004) 1–12
JOURNAL OF CATALYSIS
www.elsevier.com/locate/jcat

Characterization of WO_x/CeO_2 catalysts and their reactivity in the isomerization of hexane

A.-S. Mamede,[a] E. Payen,[a] P. Grange,[b] G. Poncelet,[b] A. Ion,[c] M. Alifanti [c] and V.I. Pârvulescu [c,*]

[a] *Laboratoire de Catalyse de Lille, UMR CNRS 8010, Université des Sciences et Technologies de Lille, 59 655 Villeneuve d'Ascq, France*
[b] *Unité de Catalyse et Chimie des Matériaux Divisés, Université Catholique de Louvain, Place Croix du Sud, 2/17, B-1348 Louvain-la-Neuve, Belgium*
[c] *Department of Chemical Technology and Catalysis, University of Bucharest, B-dul Regina Elisabeta 4-12, Bucharest 70346, Romania*

Received 21 July 2003; revised 21 November 2003; accepted 6 January 2004

Abstract

Two series of WO_x–CeO_2 catalysts with a W content between 4.0 and 12 wt% prepared by coprecipitation (CW-PP) and impregnation (CW-IMP) of CeO_2 were investigated with the aim of examining the role of tungsten and the support in acid-catalyzed reactions. The catalysts were characterized with several in situ techniques (XRD, Raman, XPS, and NH_3-DRIFT), and nitrogen adsorption at 77 K. XRD results pointed to the preferential formation of crystalline $Ce_2(WO_4)_3$ which was completed at 1173 K. Crystalline WO_3 was absent in both series of CW-IMP and -PP catalysts. Raman spectra of CW-PP catalysts suggested the possible formation of WO_3 only in the catalyst with 11.9 wt% W calcined at 1173 K. For the CW-IMP catalysts, the bands assigned to amorphous WO_3 were clearly seen in samples calcined at 1173 K, with their intensity depending on the W content. The treatment of the catalysts under hydrogen resulted in a decrease of the characteristic Raman band of ceria, and changes of the $Ce_2(WO_4)_3$ phase. NH_3-DRIFT spectra showed the presence of both Lewis and Brønsted acid sites, the strength of which increased with calcination temperature. The effect of hydrogen in improving the acidity consists either of a degradation of the $Ce_2(WO_4)_3$ phase with the formation of small WO_3 domains or of some new arrangements like Lindqvist polyanions, both species being susceptible to an easy transformation of Lewis to Brønsted acid sites. Isomerization of hexane over WO_x/CeO_2 catalysts produced mono- and di-alkylated hydrocarbons and methylcyclopentane. Increasing tungsten contents enhanced the activity and selectivity to methylcyclopentane. The presence of hydrogen improved the stability of the catalysts but decreased their activity, and resulted in important changes of the selectivity: the mono- and di-alkylated hydrocarbons predominated.

Keywords: WO_x/CeO_2; Hexane isomerization; In situ XRD; XPS and Raman; NH_3-DRIFT

1. Introduction

Branched alkanes are very important for high octane gasolines [1]. They are produced by isomerization of normal paraffins, an acid-catalyzed chain reaction which is preferably performed at low temperatures in order to avoid cracking and aromatization products and to achieve high selectivities to the isomers. The classic catalysts still used today include toxic, corrosive compounds such as sulfuric acid, halides, and oxyhalides. In order to suppress the environmental hazards that these catalysts generate, new solid acid catalysts need to be found, the challenge being to develop heterogeneous catalysts with high densities of strong acid sites, which are able to operate isomerization at low temperatures.

In accordance with these requirements, the catalyst must be able either to protonate an alkane with generation of a carbenium ion-like intermediate [2] or to accommodate metal cations or metal oxide clusters with the oxide supports in structures which stabilize the protons responsible for the Brønsted acidity [3,4]. The first category mainly corresponds to superacidic systems, and heterogeneous catalysts can only partially generate such species. Another possibility of generating such carbocations was suggested by Fărcaşiu et al. [5] for the isomerization over sulfated zirconia catalysts. These catalysts, first reported by Holm and Bailey [6], were considered as superacid solids [7], but further studies infirmed this assumption [8,9]. Fărcaşiu et al. [5] proposed an alternative mechanism consisting of a one-electron transfer from the substrate to the catalyst, followed by the cleavage of the

* Corresponding author.
E-mail address: v_parvulescu@chem.unibuc.ro (V.I. Pârvulescu).

0021-9517/$ – see front matter
doi:10.1016/j.jcat.2004.01.008

radical cation. This supposition was supported by both spectroscopic and catalytic data [10,11], and quantum-chemical calculations [12].

Despite the tremendous effort focused on sulfated zirconias, these catalysts deactivate relatively fast, mainly by coke deposition but also by loss of sulfur, and they are rather sensitive to water [13–15]. However, zirconia seems to be a rather adequate support for accommodating metal cations or metal oxide clusters, and addition of tungstate [16–21], molybdate [22], borate [23], and phosphate [24] has been found to produce relatively strong acid sites.

Tungstated zirconias (WZ) have been particularly investigated due to their interesting catalytic behavior at low temperatures. In addition to its acidity, the mesoporous structure of WZ ensures an easy transport of reactants and products which minimizes the unwanted secondary reactions which, in microporous acid solids, are favored by the restricted pore sizes and long interpellet residence times.

The catalytic behavior of these acid solids is strongly influenced by the presence of hydrogen, although the role of hydrogen is still unclear. Baertsch et al. [25] considered that hydrogen does not affect the density of the Brønsted acid sites but rather generates polytungstate WO_x domains, the density being the prevalent factor. On the basis of isotopic and chemical titration of the acid sites in WO_x domains supported on zirconia, these authors concluded that the density of the H^+ Brønsted acid sites formed from hydrogen is low, and their formation may be aided by H_2 dissociation on the ZrO_2 support. For Kuba et al. [4], the catalytic properties of WZ depend on the ability to generate W^{5+}–OH sites under reducing conditions at low temperatures. Spectroscopic measurements verified the formation of reduced W^{5+} species, suggesting a reaction mechanism much similar to that proposed by Fărcaşiu et al. [5].

In summary, these studies suggest that the isomerization reaction involves, at least in the initiation step, a redox mechanism. The catalytic properties are also directly influenced by the preparation method, reduction and calcination temperatures, and W loading [26,27]. The support may also play an important role in this redox mechanism [25]. Eibl et al. [28] investigated WO_x–TiO_2 catalysts, and their spectral and diffraction data gave a different pattern than when using ZrO_2 as a support.

With this background, the goal of this study was to collect additional evidence for the redox behavior of supported WO_x catalysts. Cerium oxide exhibits stronger oxidizing properties than ZrO_2 and, therefore, its use could elucidate the behavior of supported tungsten catalysts in the isomerization of hydrocarbons. For that purpose, CeO_2 instead of zirconia was chosen as a support. In order to eliminate the possible contribution of chlorine, which even in a very low amount may have an important influence on isomerization [29], cerium nitrate was adopted as a precursor, and hexane isomerization as test reaction.

2. Experimental

2.1. Catalyst preparation

Two series of WO_x–CeO_2 catalysts containing 4, 7.9, 9.5, and 11.9 wt% W were prepared. The first series (denoted as PP) was obtained by coprecipitation of an aqueous solution of cerium nitrate ($Ce(NO_3)_3 \cdot 6H_2O$, Fluka) and ammonium metatungstate ($(NH_4)_6H_2W_{12}O_{41} \cdot H_2O$, Riedel-de Haen) with ammonia, until reaching pH 7. The precipitates were washed, dried, crushed, and calcined for 3 h in static air at different temperatures in the range 973–1173 K using a ramp of 0.5 K min^{-1}.

The second series of catalysts (denoted as IMP) was prepared by incipient wetness impregnation of a CeO_2 support. The ceria support was prepared by decomposition (1173 K for 3 h) of cerium citrate to CeO_2 in static air (citrate method [30]). It was impregnated with 2.5 ml g^{-1} solutions containing the appropriate amounts of ammonium metatungstate. After drying, the catalysts were calcined for 3 h at 1173 K (ramp of 0.5 K min^{-1}). The ceria support calcined under those conditions had a specific surface area of 28.5 m^2 g^{-1}.

2.2. Catalyst characterization

Chemical analysis of the catalysts was performed by ICP-AES. The W contents are given in Table 1.

The BET specific surface areas and the pore size were obtained from nitrogen adsorption isotherms recorded at 77 K with an ASAP 2000 instrument from Micromeritics. The samples were outgassed at 423 K for 12 h under a residual pressure of 0.1 Pa. The surface areas of the catalysts are indicated in Table 1.

XRD patterns were recorded with a D5000 Kristalloflex diffractometer from Siemens using the Cu-K_α radiation ($\lambda =$ 1.5418 Å). Data acquisition was done in the 2–65° 2θ range, with a scan step of 0.03°. In situ variation of the crystallinity was monitored on the same apparatus, using a standard furnace disposed in the analysis chamber. The freshly dried precursor powders (40–75 μm) were mounted on a Pt sample holder and heated between room temperature and 1173 K at a rate of 1 K s^{-1}, the patterns being recorded between 20 and 55° 2θ (scan step of 0.03°) after a stabilization period for 1 h at different temperatures.

XPS spectra were scanned at room temperature on a SSX-100 spectrometer, Model 206 from Surface Science Instrument. The pressure in the analysis chamber during the analysis was 1.33 mPa. Monochromatized Al-K_α radiation ($h\nu = 1486.6$ eV) was used. It was generated by bombarding the Al anode with an electron gun operated with a beam current of 12 mA and acceleration voltage of 10 kV. The spectrometer energy scale was calibrated using the Au $4f_{7/2}$ peak centered at 83.98 eV. Charge correction was made with the C 1s signal of adventitious carbon (C–C or C–H bonds) located at 284.8 eV. The composite peaks were decomposed

Table 1
Surface areas and apparent tungsten density of the investigated catalysts, calcined at 1173 K

Catalyst	Preparation procedure					
	PP			IMP		
	W content (wt%)	Surface area ($m^2\,g^{-1}$)	W density ($W_{atoms}\,nm^{-2}$)	W content (wt%)	Surface area ($m^2\,g^{-1}$)	W density ($W_{atoms}\,nm^{-2}$)
CW4.0	3.96	19.6	3.01	3.96	16.8	4.5
CW7.9	7.93	16.3	5.65	7.93	14.5	9.1
CW9.5	9.52	14.0	7.6	9.52	11.8	10.9
CW11.9	11.89	14.0	8.23	11.89	10.8	13.7
CeO_2	–	26.7	–	–	28.5	–
CeO_2–H_2O[a]	–	–	–	–	28.5	–

[a] CeO_2 calcined for 3 h at 1173 K, impregnated with water, and recalcined at 1173 K for another 3 h.

by a fitting routine included in the ESCA 8.3 D software. The atomic surface compositions were calculated using the sensitivity factors provided with the ESCA 8.3 D software, applied to the surface below the corresponding fitted XPS signals.

NH_3-DRIFT (diffuse reflectance infrared Fourier transform) spectra were collected with a Brucker IFS88 spectrometer (200 scans with a resolution of 4 cm^{-1}). Pure samples were placed inside a commercial controlled environmental chamber (Spectra-Tech 0030-103) attached to a diffuse reflectance accessory (Spectra-Tech collector). The stability of the adsorbed ammonia species during the increase of temperature was investigated by recording the spectra under flowing helium (30 $ml\,min^{-1}$) at room temperature, 373, 473, and 573 K, after exposure to an ammonia flow (30 $ml\,min^{-1}$) for 30 min at room temperature.

The Raman spectra were recorded on a LabRAM Infinity spectrometer (Jobin Yvon) equipped with a liquid nitrogen detector and a frequency-doubled Nd:YAG laser supplying the excitation line at 532 nm. The spectrometer was calibrated using the silicon line at 521 cm^{-1}.

For in situ Raman analysis, the samples were placed in a temperature- and atmosphere-controlled stainless-steel cell directly adapted to the XY manual stage of the Raman microscope. The powder samples were deposited on a sintered glass disk which could be heated up to 773 K by an electrical resistor coil surrounding the sample holder. The optically polished Pyrex window of the cell was 1.8 mm thick. Sample illumination and light collection proceeded with a 50 long frontal objective. The power at the sample surface was below 5 mW.

2.3. Catalysis

The catalytic activity was evaluated in a conventional installation, over 50 mg of catalyst powder loaded in a tubular, down-flow-operated quartz microreactor. Hexane was passed through the catalyst bed at a space velocity of 120 $cm^3\,g_{cat}^{-1}\,h^{-1}$. The reaction was performed at temperatures in the range 393–453 K, both in the absence and in the presence of hydrogen (30 $ml\,min^{-1}$). Analysis of the products was achieved in a Varian Star 3400CX gas chromatograph equipped with a Chrompack 7530 capillary column (WCOT fused-silica column with CP-Sil PONA CB stationary phase). The presence of alkenes (i.e., hexenes) as established by chromatography was confirmed by hydrogenation treatment at 343 K for 4 h of the liquid effluent in a stainless-steel autoclave on a Pd–Li/Al_2O_3 catalyst: only alkanes were found. The catalytic activity was expressed as transformation rate of hexane and selectivity to dimethylbutane and methylcyclopentane.

3. Results

3.1. Textural and structural characterization

All the catalysts developed a specific surface area between 10 and 20 $m^2\,g^{-1}$ (Table 1), which is relatively high for the calcination temperature used (1173 K). All the catalysts contained mesopores (i.e., larger than 4 nm). For both series of catalysts, the increase of the W content brought about a continuous decrease of the specific surface area which, for a tungsten loading of 11.9 wt%, represented about half that of the support alone (Table 1). The impregnated (-IMP) catalysts exhibited slightly smaller surface areas than the corresponding -PP catalysts. The smaller surface areas of both series of catalysts than of the support are strictly due to the presence of W species at the surface, likely located at the entrance of the pores. No morphological change was observed after rehydration of the support (to simulate the impregnation conditions), followed by recalcination.

The structural changes occurring with increasing calcination temperature are shown in Fig. 1 for the CW9.5-PP catalyst. The XRD patterns of the CW-PP catalysts exhibited only two phases, which appeared distinctly as temperature increased. They corresponded to CeO_2 with the cerianite structure (JCPD-ICDD 43-1002), and $Ce_2(WO_4)_3$ (JCPD-ICDD 31-0340) [31]. The reflections of the $Ce_2(WO_4)_3$ phase were well defined at 1123 K, and the crystallization process was completed at 1173 K (Fig. 1). Interestingly, the CW-IMP samples (Fig. 2) exhibited the same features as the CW-PP samples calcined at 1173 K, namely, the presence of only two phases, regardless of the W loading, without any

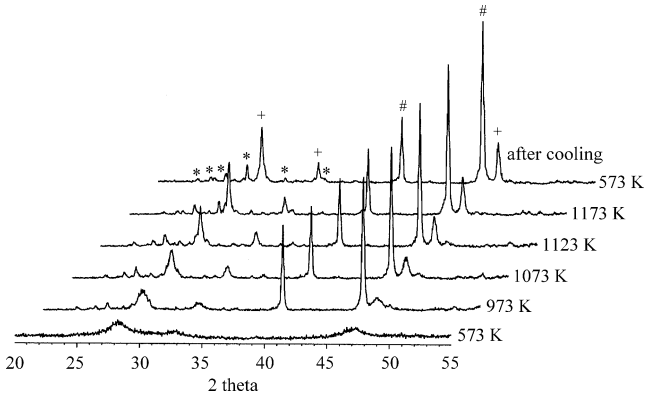

Fig. 1. XRD patterns at increasing and decreasing temperatures of PP 9.5-C: (∗) $Ce_2(WO_4)_3$; (+) CeO_2; (#) Pt sample-holder reflections.

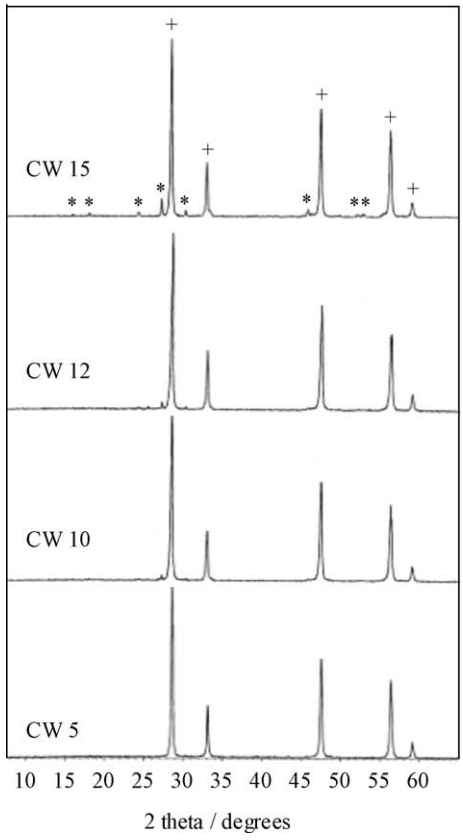

Fig. 2. XRD pattern of CW-IMP catalysts calcined at 1173 K: (∗) $Ce_2(WO_4)_3$, (+) CeO_2.

X-ray-detectable trace of tungsten oxides. Actually, the formation of the $Ce_2(WO_4)_3$ phase occurred as a solid–solid reaction between the in situ formed CeO_2 and WO_x [32].

The density of superficial tungsten was calculated from two different approaches. For the impregnated samples, an apparent W surface density was calculated as the ratio between the W atom content per gram of sample and the measured area of the CeO_2 support obtained using the citrate method (Table 1). For the CW-PP samples, the apparent W density was calculated using the size of $Ce_2(WO_4)_3$ established from the X-ray reflection at 27.36° 2θ [31] assuming that these particles approximate a sphere (Table 1). The values of Table 1 indicate that there was a dependence between the tungsten loading and the W density at the surface. The relationship was linear with distinct slopes according to the preparation method. Table 1 also shows that the CW-IMP catalysts had a higher W density.

3.2. X-ray photoelectron spectroscopy

The results of the XPS investigation of the catalysts calcined at 1173 K are compiled in Table 2. Independent of the preparation method, the W $4f_{7/2}$ and Ce $3d_{5/2}$ levels had binding energy values included in very narrow ranges, namely, 35.5–35.8 and 882.5–882.7 eV, respectively. The first range corresponded to W^{6+} [33], while for Ce, the spectrum (Fig. 3) exhibited mainly the peak characteristic of the support (Ce^{4+}) [34]. The shoulders at 885 and 905 eV, values corresponding to $Ce_2(WO_4)_3$ (Ce^{3+}), might indicate a partial reduction of cerium in the presence of tungsten. The literature noted that because of the complex features of the Ce 3d region, it is very difficult to assess the presence of Ce^{3+} from changes in the 885–905 eV region and, in accordance, only the decrease of the peak at 916.7 eV could be a probe for determining the presence of reduced species [35,36]. Treating the samples in flowing hydrogen (30 ml min^{-1}) for 2 h at 513 K (the highest reaction temperature) did not bring major changes to the XPS spectra. Ce was slightly more reduced as observed by the increase of intensity of the aforementioned shoulders.

At the same time, the binding energy of the O 1s level was shifted by 0.6–0.8 eV to higher values with respect to pure CeO_2, also pointing to a direct contribution of tungsten-containing species. It should be noted that the O 1 s signal was symmetric, which suggests a homogeneous superficial composition.

Table 2
XPS investigation results

Catalyst	W $4f_{7/2}$ BE (eV)		Ce $3d_{5/2}$ BE (eV)		O 1s BE (eV)		W/Ce atomic ratio		
	PP	IMP	PP	IMP	PP	IMP	Chemical	PP	IMP
CW4.0	35.6	35.6	882.6	882.5	529.8	529.8	0.04	0.37	0.47
CW7.9	35.6	35.8	882.5	882.7	529.8	530.0	0.08	0.53	0.41
CW9.5	35.6	35.7	882.6	882.6	530.1	529.9	0.10	0.59	0.43
CW11.9	35.5	35.8	882.5	882.7	530.0	529.9	0.13	0.45	0.37
CeO_2	–	–	882.2		529.2		–	–	–

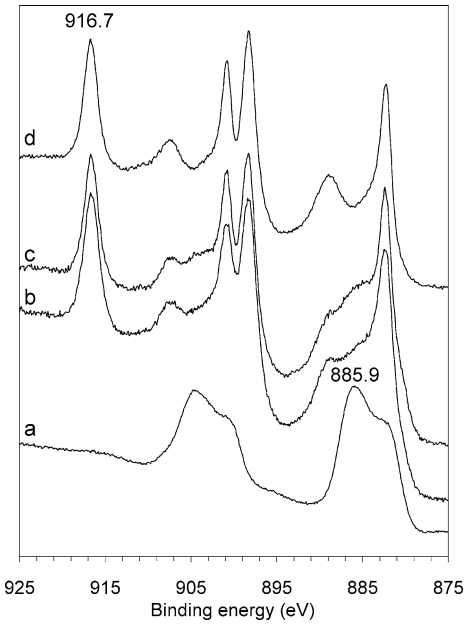

Fig. 3. XPS spectra of the Ce 3d level of (a) $Ce_2(WO_4)_3$, (b) CW9.5-PP, (c) CW9.5-PP after H_2 reduction at 300 °C, and (d) CeO_2.

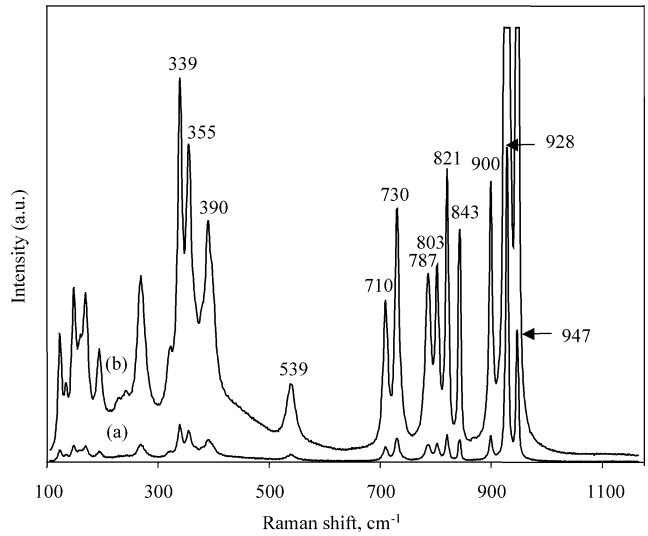

Fig. 4. Raman spectra of Ce(III) tungstate. Acquisition time: (a) 1 s and (b) 10 s.

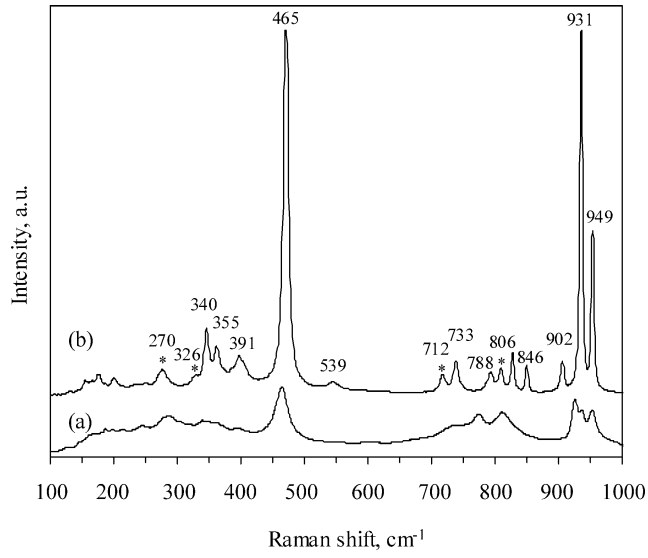

Fig. 5. Raman shift for CW4.0-IMP calcined at 973 K (a) and 1173 K (b).

The results of Table 2 also point to a W surface enrichment for all the catalysts. Since the W contents of the -PP and -IMP catalysts were very close to each other, both series are therefore considered simultaneously, as shown in Table 2. The XPS W/Ce ratios were 3–6 times higher than the values calculated from the chemical analysis, depending on the preparation method and W loading. It would be speculative to compare the dispersion of W from these measurements. If a high surface content of W (thus a high W/Ce atomic ratio) could be expected for the -IMP catalysts, it must be supposed from the high W/Ce ratios of the -PP catalysts that the W-containing species segregated preferentially at the surface. But during the impregnation, from results from the calculated W superficial density (Table 1), several layers of tungsten might be formed, and thus many W atoms became silent.

3.3. Raman spectroscopy

Raman spectroscopy gave additional structural information on the tungsten species in these catalysts. Crystalline WO_3 has a distorted ReO_3 structure, made of corner-shared $[WO_6]$ groups. The Raman spectrum exhibits three main lines at 806, 714, and 271 cm^{-1}, assigned to W–O stretching modes (A_{1g}, E_g) and W–O–W bending mode (F_{2g}), respectively.

With respect to the $Ce_2(WO_4)_3$ species, the formation of which at the higher temperatures was established by XRD, no Raman data on this compound have been found in the literature. In order to help in the interpretation for these results, the Raman spectrum of Ce(III) tungstate (Interchim) was also reported (Fig. 4). In the isopolytungstate species, the W exhibits a distorted octahedral geometry with generally more $WO_{2(t)}$ groups, where t stands for terminal oxygen atom. The symmetric and antisymmetric stretching modes of these groups are observed at 960–980 and 900–920 cm^{-1}, respectively. A comparison of the $Ce_2(WO_4)_3$ and WO_3 references clearly shows the difference between the structure of $[WO_4]$ and $[WO_6]$ units: the most intense line is observed at higher wavenumbers for the tetrahedral unit (around 900 cm^{-1}) relative to the octahedral unit (806 cm^{-1}). In the isopolytungstate species, which consist of more or less distorted edge or corner shared octahedral units, the most intense Raman line is observed around 960–980 cm^{-1} and assigned to the symmetric stretching vibration modes of the $WO_{2(t)}$ groups, where t stands for terminal oxygen atoms.

Raman spectra of CW11.9-IMP recorded at two calcination temperatures are compared in Fig. 5. The catalyst calcined at 973 K exhibited a line at 460 cm^{-1} assigned

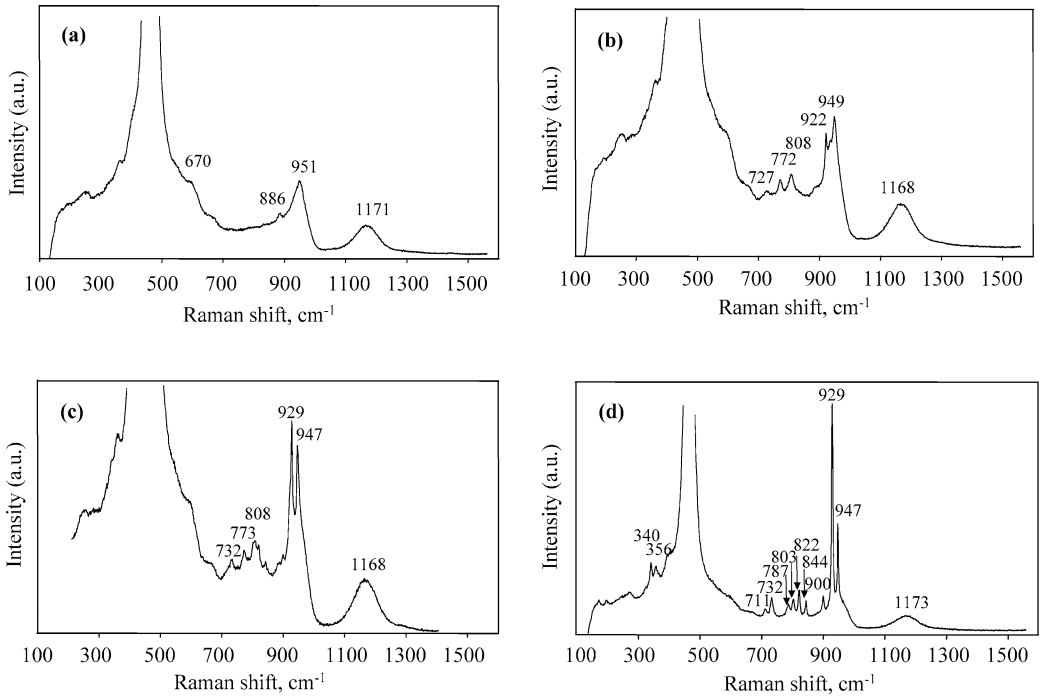

Fig. 6. Raman spectra of the PP-WO_x/CeO_2 under ambient conditions: (a) CW 4.0; (b) CW 7.9; (c) CW 9.5; (d) CW 11.9 (* CeO_2 support).

to crystalline ceria (E_g mode) [37]. The broad band between 700 and 850 cm^{-1} can be assigned to the presence of amorphous WO_3 oxide, and the two sharper lines in the region 900–950 cm^{-1}, to W=O_t stretching modes of isopolytungstate species [38,39]. The increase of calcination temperature resulted in a much better defined structure as inferred from the sharp lines in the region of oxotungstate species. This spectrum is characteristic of the $Ce_3(WO_4)_3$ compound (Fig. 5, spectrum b). This latter spectrum (sample calcined at 1173 K) will be discussed in more detail. It contains lines of WO_3 (at 270, 326, 712, and 806 cm^{-1}), $Ce_2(WO_4)_3$ (340, 355, 391, 821, 846, 902, 931, and 949 cm^{-1}), and CeO_2 (at 465 cm^{-1}). The intensity of the lines assigned to these species increased parallel to the W content.

The Raman spectrum of CW4.0-PP (Fig. 6a) exhibited a broad line at 951 cm^{-1} and a shoulder at 886 cm^{-1}, which is assigned to a well-dispersed polytungstate phase, whereas the spectrum of CW7.9-PP (Fig. 6b) had sharp lines at 949 and 922 cm^{-1}, and three smaller lines at 808, 772, and 727 cm^{-1}. The line at 1168–1173 cm^{-1} corresponds to CeO_2. The Raman spectrum of CW11.9-PP (Fig. 6d) contained two sharp lines at 947 and 929 cm^{-1} and seven smaller features at 900, 844, 822, 803, 787, 732, and 711 cm^{-1}. This spectrum can be considered as characteristic of a well-crystallized $Ce_2(WO_4)_3$ compound. Only in the case of CW11.9-PP (Fig. 6d), the lines at 803, 711, and 272 cm^{-1} could also be ascribed to WO_3. It is likely that segregated WO_3 particles could also exist at lower loadings, but probably in too small amounts as to be detected by XRD and Raman spectroscopy. At intermediate W loading (CW7.9-PP or CW9.5-PP), both entities, i.e., the isopolytungstate and the $Ce_2(WO_4)_3$ compound, should be present to explain the modifications of the Raman spectrum in the 930–959 cm^{-1} spectral range. As the Raman microprobe allows us to analyze selected particles, a heterogeneity is observed for the CW11.9-PP. Indeed, depending on the particles, the spectrum of this sample may correspond to the one observed at intermediate W loading or to the well-defined cerium tungstate compound.

In summary, bands at 922–929 and 803–808 cm^{-1} attributed to oxotungstate species are observed in the Raman spectra of CW7.9–11.9-PP (Figs. 6b–6d) and are associated with tetrahedral [WO_4] units. The other Raman bands are likely due to distortions which induce a lowering of the symmetry. These results are consistent with those of Yu et al. [40] who reported in situ Raman spectra of 30 mol% Na_2WO_4/CeO_2 maintained at high temperatures (773–923 K) in flowing helium, with bands at 304, 804, and 921 cm^{-1} corresponding to the E, F_2, and A_1 fundamental modes of Na_2WO_4.

These results completed the image obtained by in situ XRD, namely, that with increasing W loading and upon calcination at high temperature, the $Ce_2(WO_4)_3$ compound was formed. At lower loadings, the Raman spectrum (main band at 951 cm^{-1}) was characteristic of polytungstate species well dispersed on the ceria support [41,42].

3.4. In situ RAMAN spectra recorded in hydrogen atmosphere

The behavior under reducing conditions was studied in order to identify possible intermediate species that could be formed during isomerization in the presence of hydrogen.

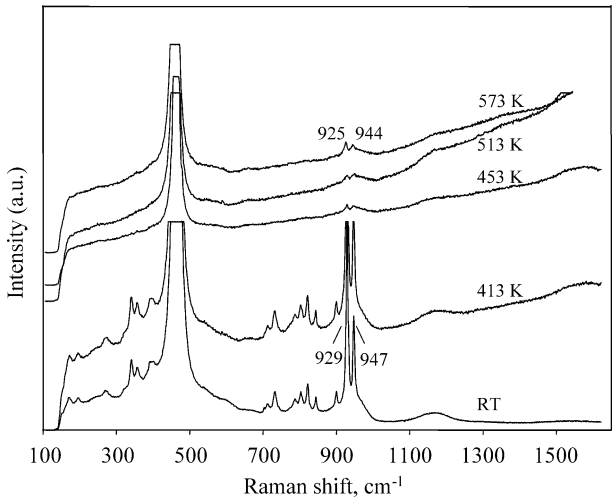

Fig. 7. In situ Raman spectra of CW7.9-PP after H_2 reduction (2 h) at different temperatures; acquisition time 120 s (413, 453 K) and 60 s (513, 573 K).

Raman spectra were recorded after a treatment for 2 h under flowing hydrogen (30 ml min^{-1}) at different temperatures in the 413–573 K range.

As shown in Fig. 7, the intensity of the characteristic band of ceria decreased with increasing temperature, and its position shifted from 464 to 460 cm^{-1} at the highest reduction temperature. This behavior is typical of all the investigated samples, regardless of their W content. The decrease of the intensity of the bands due to the cerium tungstate phase can be assigned to its transformation upon the reduction treatment. Important changes also occurred in the region of the WO_x bands. At the higher temperatures, the lines characteristic of the well-defined compound (929–947 cm^{-1}) strongly decreased for all the investigated samples, regardless of their W content.

For the CW-IMP-samples (figure not shown), the increase of the W loading resulted in a drastic loss of intensity of the ceria bands, associated with prominent bands characteristic of the polytungstate species. The increase of the band intensity of the polytungstate species with increasing W loading ran parallel to the change of the tungsten density.

3.5. NH_3-DRIFT spectra

NH_3-DRIFT spectra recorded at increasing temperatures showed bands of ammonia adsorbed both on Brønsted (1449–1384 cm^{-1}) and Lewis (1597–1530 cm^{-1}) acid sites. A broad band in the range 2500–3500 cm^{-1} was also present in the spectrum recorded at room temperature (range not shown), resulting from contributions of the ν_{as}(N–H), ν_s(N–H), $2\delta_{as}$(H–N–H), $2\delta_s$(H–N–H), and δ_{as}(H–N–H) modes of ammonia adsorbed on Lewis acid sites of the surface [43]. The samples calcined in air at 973 or 1173 K exhibited only one band at 1430 cm^{-1} due to ammonia adsorbed on Brønsted acid sites, independent of the way the catalysts were prepared (CW-PP or CW-IMP).

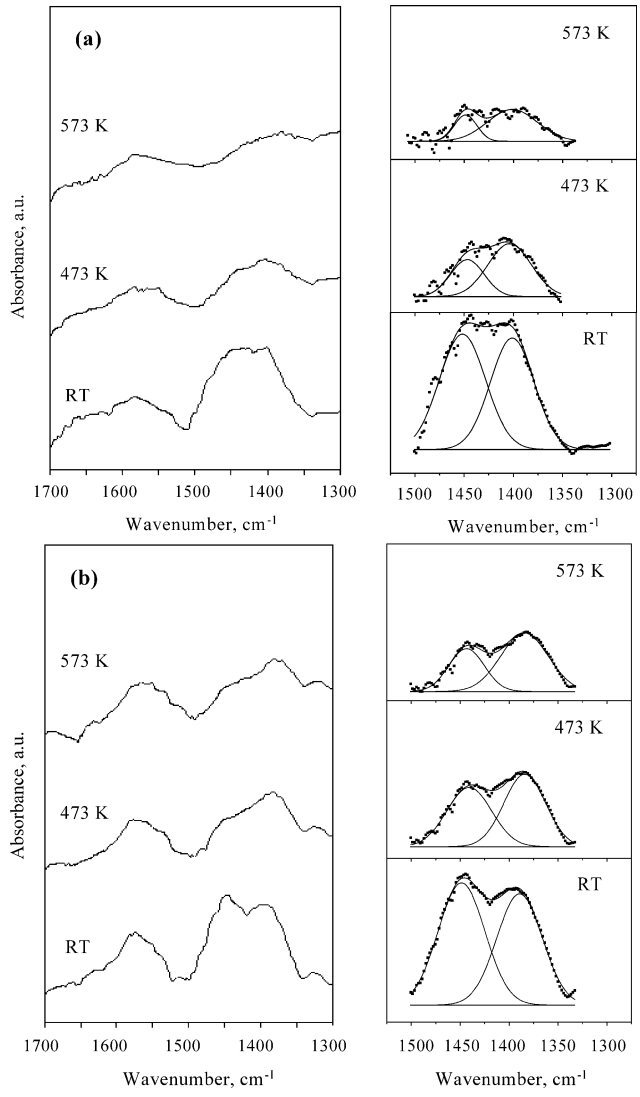

Fig. 8. NH_3-DRIFT spectra taken at different temperatures for (a) CW4.0-PP and (b) CW7.9-PP calcined at 1173 K and pretreated in H_2 at 513 K.

In contrast, the samples previously treated in hydrogen at 513 K for 3 h showed two bands assigned to ammonia adsorbed on Brønsted acid sites, namely, at 1446 and 1408 cm^{-1} for the samples calcined at 973 K, and at 1449 and 1384 cm^{-1} for those calcined at 1173 K. These bands could be assigned to (NH_4^+) adsorbed species. Since the δ_{asym} in (NH_4^+) free ion is a triply degenerated mode, a change in the symmetry due to its surface coordination may induce band splitting. The increase of the calcination temperature of the samples from 973 to 1173 K was also consistent with an increase of the number of acid sites, as inferred from the intensity of the bands associated with ammonia adsorbed on both the Brønsted and the Lewis acid sites. The splitting was also clearer. The increase of the desorption temperature to 573 K resulted in a logical decrease of the intensity of these bands.

Figs. 8a and 8b show the effect of the W loading on the acidity. To make this influence clearer, the spectra

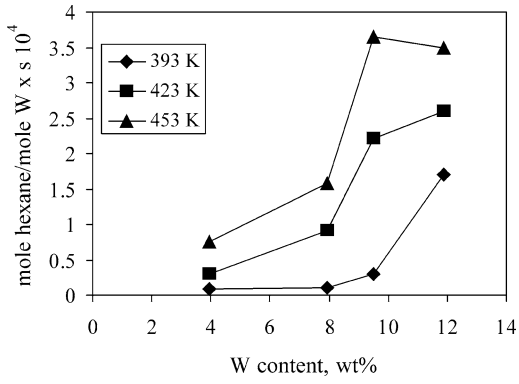

Fig. 9. Catalytic activity of CW-PP catalysts.

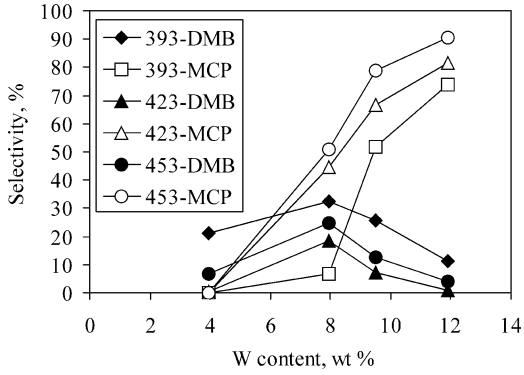

Fig. 10. Selectivity to dimethylbutanes (DMB) and methylcyclopentane (MCP) on CW-PP catalysts (conversion: 20%).

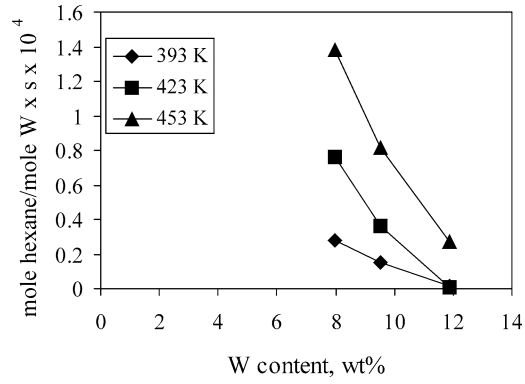

Fig. 11. Catalytic activity of CW-IMP catalysts as a function of W loading.

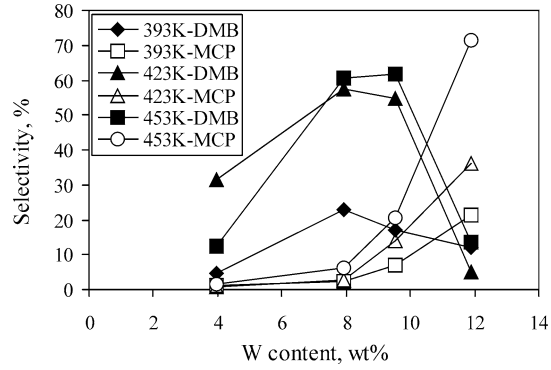

Fig. 12. Selectivity to dimethylbutanes (DMB) and methylcyclopentane (MCP) on CW-IMP (conversion: 20%) vs W loading.

were reconsidered by fitting the results in the region 1350–1500 cm^{-1}. The comparative analysis of these spectra indicated that the increase of the W loading led to an increased number of acid sites. Also the strength of these sites appeared to be slightly enhanced by the content of W, as inferred from the comparison of the desorption spectra at 573 K.

The NH_3-DRIFT spectra collected for CW-IMP samples previously treated in hydrogen (spectra not shown here) also suggested the presence of a second population of Brønsted acid sites, but only for the samples calcined at 1173 K, and in a much smaller amount. Contrary to the CW-PP catalysts, the increase of the W loading corresponded to smaller bands, suggesting less acid sites.

3.6. Catalytic activity in the absence of hydrogen

The catalytic performances of the PP catalysts in *n*-hexane isomerization are shown in Fig. 9. All the catalytic runs were performed over 50 mg catalyst, using a space velocity of 2×10^{-3} ml min^{-1} mg^{-1}. As a general tendency, the activity increased with increasing W loading and reaction temperature. At 393 K, the activity was rather low, except for CW11.9-PP, which exhibited some activity. At 423 and 453 K, the activity increased, with small differences between CW9.5-PP and CW11.9-PP.

The main reaction products were the mono- and di-alkylated isomers, and methylcyclopentane. The selectivity to these compounds depended on both reaction temperature and W loading (Fig. 10). Over CW4.0-PP, the mono-alkylated isomers predominated (not shown in the figure), irrespective of temperature. Hydrogen and small amounts of alkenes (1- and 2-hexenes) were formed in all the experiments. A subsequent hydrogenation of the reaction products confirmed the presence of hexenes since they were completely hydrogenated. With increasing W loading, except for CW7.9-PP at 393 K, methylcyclopentane was the major product.

The CW-IMP catalysts showed a different activity. They were substantially less active than the CW-PP samples and, in contrast, an increase of the W content gave less performing catalysts (Fig. 11). These data correlate well with NH_3-FTIR results which indicated that the increase of the W loading corresponded to smaller bands, suggesting less acid sites. However, the variation of the reaction products as a function of temperature and W loading showed a similar behavior (Fig. 12). As for the CW-PP catalysts, hydrogen and alkenes were formed in all the reactions, and an increase of the W loading improved the selectivity to methylcyclopentane, with mono-alkylates being predominant at low temperature.

Time-on-stream experiments showed that this level of activity was preserved over a relatively short period: after

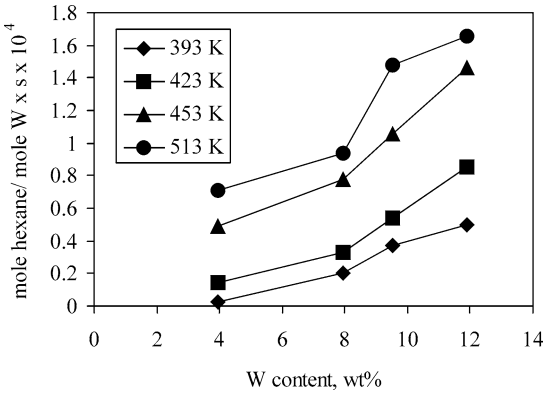

Fig. 13. Catalytic activity of CW-PP catalysts in the presence of H_2.

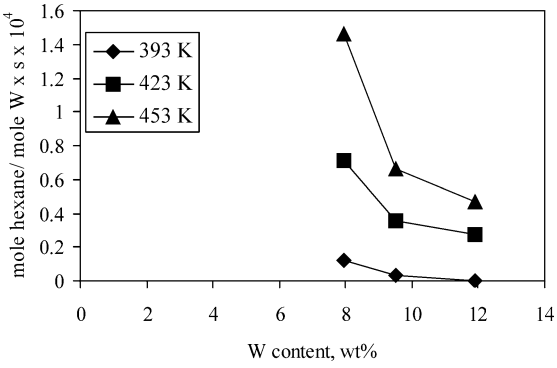

Fig. 14. Catalytic activity of CW-IMP catalysts in the presence of H_2.

90 min, the activity diminished near to zero and the color of the catalysts turned from white to brownish as a result of coke deposition. As expected, there was a direct relationship between deactivation and maximum level of activity. The reaction required an induction period which also was in direct relation with the activity, i.e., with temperature and tungsten loading.

3.7. Catalytic activity in the presence of hydrogen

Experiments carried out under hydrogen showed that the maximum of activity was reached after an induction period about half that in the absence of hydrogen. Also, the presence of hydrogen diminished the activity of the catalysts (compare Figs. 9 and 11 with Figs. 13 and 14), irrespective of their preparation mode, but improved significantly the stability of the catalysts: after 3 h on stream, the activity level was nearly unchanged and the catalyst preserved its white color. The activity of the CW-PP catalysts increased with increasing tungsten loading and temperature, while over the CW-IMP catalysts, the activity increased with increasing reaction temperature, but decreased with increasing W loading (Figs. 13 and 14).

The presence of hydrogen also brought about changes of the selectivity of the CW-PP catalysts and, compared with trials without hydrogen, these changes occurred for W loadings higher than 7.9 wt% (Fig. 15). Over CW4.0-PP, the

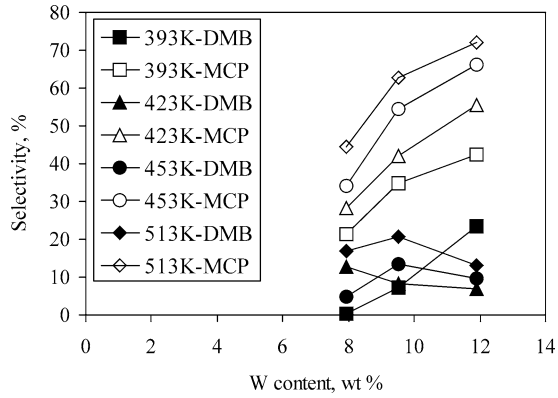

Fig. 15. Selectivity to dimethylbutanes (DMB) and methylcyclopentane (MCP) on CW-PP catalysts in the presence of H_2 (conversion 20%).

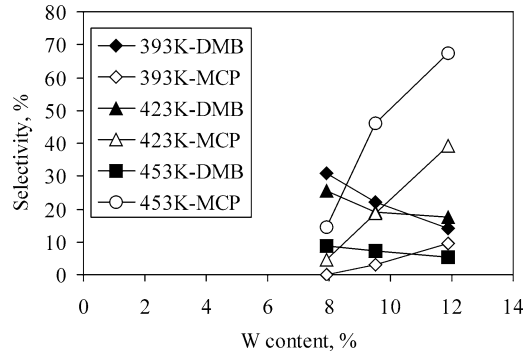

Fig. 16. Selectivity to dimethylbutanes (DMB) and methylcyclopentane (MCP) on CW-IMP catalysts in the presence of H_2 (conversion 20%).

mono-alkyl isomers were the main reaction products (not shown in the figure). The increase of the W loading to 7.9 and 9.5 wt% was accompanied by a change of the selectivity, and, except at 293 K where the mono-alkyls still were the major products, the di-alkyl isomers predominated. For CW11.9-PP, depending on the reaction temperature, the main products were either the mono-alkylated isomers (at low temperatures) or methylcyclopentane (at high temperatures). For the CW-IMP catalysts, the variation of the selectivity followed a similar trend as in the absence of hydrogen, namely, at low temperatures favored the mono-alkylated isomers whereas, at high temperatures, methylcyclopentane was the main reaction product (Fig. 16).

4. Discussion

4.1. Catalysts structure

WO_x/CeO_2 catalysts prepared by coprecipitation and impregnation led to solids with comparable textural and structural features, and with surface areas between 10 and 20 $m^2\,g^{-1}$ depending on the tungsten content. According to the W loading, the apparent surface density of W corresponded to values in the range 4.5–14 W atoms nm^{-2} for the CW-IMP catalysts, and 3–8 W atoms nm^{-2} for the CW-

PP ones. Neither the water used for the impregnation, nor a second calcination had an influence on the textural and structural properties of CeO_2 used as support for the impregnation.

XRD results pointed to the preferential formation of a definite crystalline tungsten compound, $Ce_2(WO_4)_3$, which does not occur when ZrO_2 or TiO_2 are used as supports [27,28,44]. For ZrO_2-supported WO_x catalysts, only isopolytungstate species were formed. No compound like $Zr(WO_4)_2$ was detected, even after a calcination at 1073 K. It has been suggested that the formation of dispersed isopolytungstate species occurred via an anion exchange or condensation reaction of tungstate anions with surface OH groups of hydrated ZrO_2 [3]. In the case of TiO_2-supported WO_x, crystalline WO_3 only appeared at temperatures higher than 973 K [28]. For lower temperatures, tungsten ions were well dispersed and incorporated to the anatase structure [28]. Alumina support generates, at low WO_x coverages, typical compounds like $Al_2(WO_4)_3$ [38]. The enhanced Lewis acidity in these catalysts was associated with isolated tetrahedral tungstate groups. But, at high coverages, the formation of distorted tungsten oxide octahedra was also observed by XANES measurements [38].

An almost unanimous conclusion upon supporting WO_x on various supports is that the catalyst must be calcined at least at 973 K to exhibit acidic properties. In situ XRD patterns indicated that a crystalline phase identified as $Ce_2(WO_4)_3$ was formed at increasing temperatures, with the completion of the crystallization process being achieved at 1173 K, namely, a temperature close to those at which active isomerization catalysts are obtained [27,44]. The absence of the XRD reflections of WO_3, even in the CW-IMP samples, is, however, surprising. Two possibilities can be invoked to explain this behavior: the WO_x clusters were too small as to be detected by XRD, or part of the tungsten ions might remain incorporated in the cerianite or $Ce_2(WO_4)_3$ frameworks, as in the case of anatase [28].

Raman spectra recorded during calcination of these materials provided some additional evidence for interactions occurring between ceria and tungsten, in support of the above speculations. For the CW-PP catalysts, bands associated to the tetrahedral [WO_4] units were detected only in the spectra of CW7.9-PP and CW11.9-PP. Raman spectroscopy suggested the presence of WO_3 entities only in the CW11.9-PP. This behavior is very similar to that of alumina-supported tungsten, where polytungstate clusters are formed only for high coverages [38]. The situation was different for the CW-IMP samples where WO_3 was present in the spectra of the samples calcined at 1173 K, with the intensity of the bands increasing with increasing W content. Also, the enhancement of the tungsten content was accompanied by a decrease of the band assigned to the support, as a result of multilayer deposition of WO_x (corresponding to nearly 14 W atoms nm^{-2} for 11.9 wt% W). There was no clear evidence for the presence of WO_3 species at lower calcination temperatures.

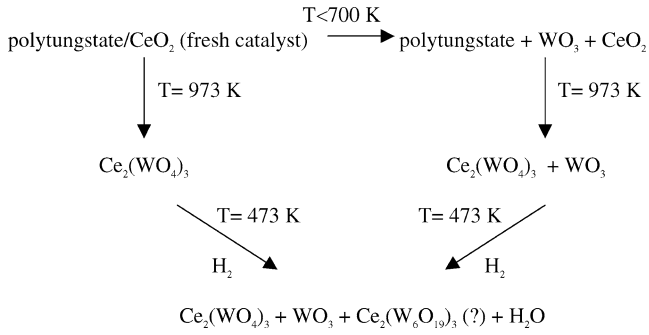

Scheme 1. Transformations in the WO_x/CeO_2 system with temperature and in hydrogen.

In situ Raman spectra of the catalysts treated under hydrogen showed a decrease of the characteristic band of ceria and changes in the $Ce_2(WO_4)_3$ phase. It is worth noting that the oxotungstate phase was still present even after this treatment. XPS analyses of these samples showed that tungsten existed as W^{6+} species, while cerium was slightly reduced. Treating these catalysts under hydrogen caused a shift of the peaks assigned to the Ce $3d_{5/2}$ level, indicative of more reduced species. Almost no change occurred in the W $4f_{7/2}$ peak, consistently with the Raman measurements. Of course, if a small part of W^{6+} were reduced to W^{5+}, both Raman spectroscopy and XPS were not sensitive enough to detect such species.

Scheme 1 describes the transformations occurring in this system.

XPS also confirmed the partial aggregation of W-containing species. This aggregation depended on the preparation route, with the CW-IMP samples being more aggregated.

4.2. Acidic properties

Both Lewis and Brønsted acid sites were observed in NH_3-DRIFT spectra, the number of which increased with calcination temperature. Indeed, the bands assigned to ammonia adsorbed on the acid sites remained after heating at 573 K only when the samples had been previously calcined at 1173 K. The pretreatment of these samples under hydrogen led to a splitting of the band assigned to ammonia adsorbed on the Brønsted acid sites, which may indicate a change in the coordination state of NH_3 on the chemisorption site. The higher frequency suggested that part of these new acid sites were stronger than in the nonreduced catalysts. Since the intensity of this band increased with increasing W content, it could be that these acid sites were related to the species generated upon the transformation of $Ce_2(WO_4)_3$, as suggested in the Raman spectra recorded in the presence of hydrogen.

It may be proposed that the Lewis acid sites could correspond to W=O species, and the Brønsted sites, to hydrogen attached to tetrahedral tungstate groups in $Ce_2(WO_4)_3$ or to distorted octahedral groups in WO_3. The increase of the Brønsted acidity with increasing W loading in the CW-PP

catalysts could hardly be related to an increased participation of WO_3. Indeed, this phase has been clearly detected only for CW-IMP catalysts which were less performing than the CW-PP ones. Another possible model is close to the one proposed by Scheithauer et al. [21] in which the active site is a Zr-heteropolytungstate with H^+ as the charge-compensating species. In the case of Ce, it is difficult to consider the formation of equivalent compounds, Ce being too large to be incorporated in a Keggin structure. Its presence as a counterion in a structure like a tungsten Lindqvist polyanion [45] would be more probable, although the existence of this polyanion cannot be proved since no band near 992 cm^{-1} has been detected in the Raman spectra. However, a very small amount of this species at the surface could not be excluded.

It thus appears that the effect of hydrogen in improving the acidity of these catalysts consists either of a degradation of the $Ce_2(WO_4)_3$ phase with the formation of small, poorly defined WO_3 domains, or perhaps other structures like Lindqvist polyanions [45], both species being equally able to undergo an easy transformation from Lewis to Brønsted acid sites. The decrease of the activity (per gram of catalyst) in the presence of hydrogen might be interpreted in similar terms, with the agglomeration of tungsten leading to a decrease of the active sites and, hence, of the turnover. The role of the support in avoiding the agglomeration of tungsten species seems to be crucial. This process is facilitated by the redox behavior of Ce. In the case of impregnated species, because of the limited interaction of cerium and tungsten, this process would take place to a smaller extent.

4.3. Catalytic behavior

In general terms, isomerization of hexane over WO_x/CeO_2 catalysts led to mono- and di-alkylated hydrocarbons and methylcyclopentane. The increase of the tungsten content brought about an increase of the activity and selectivity to methylcyclopentane. For the CW 4.0 catalysts, the main reaction products were the mono-alkylated hydrocarbons. When the reaction was carried out in the absence of hydrogen, a relatively rapid deactivation of the catalysts occurred. Introduction of hydrogen improved the stability but caused a decrease of the catalyst activity. These results suggest that the key point is the formation of alkenes. In the presence of hydrogen, the alkenes were less abundant and, consequently, the activity was decreased. Furthermore, methylcyclopentane is supposed to appear after the alkenes are formed. The presence of hydrogen also resulted in important changes of the selectivity: the mono- and di-alkylated hydrocarbons predominated. Methylcyclopentane became the majoritary product only over the catalysts with 11.9 wt% W and at high temperatures.

The correlation of the catalytic data with the characterization results obtained with various in situ techniques suggest that the behavior of these catalysts involves, as a first step, an oxidative hydride abstraction, occurring on Lewis sites associated with W=O species, followed by isomerization either as a cooperative effect on the Brønsted acid sites created by tungsten, or even on the same Lewis site from which the hydride ion was abstracted.

The increase of the selectivity to methylcyclopentane with increasing W content actually stems from an enhancement of the oxidative properties of the catalysts, parallel to the increase of the tungstate and probable WO_3 species of the catalysts. A less oxidative behavior is consistent with the isomerization of hexane to methylpentanes or dimethylbutanes. In the presence of hydrogen, part of the species which are able to abstract hydride are transformed into presumed Ce-Lindqvist-like polyanion species, decreasing the abstraction capacity and, hence, the activity. Also, these species exhibit less oxidative properties and, as a direct consequence, the dehydroisomerization to methylcyclopentane is possible only at high W contents and higher temperatures.

From results of the characterization of these catalysts using XRD, XPS, and Raman measurements, the role of the support consists of increasing the oxidative properties of tungsten. Both XPS and Raman data indicated that in the presence of tungsten ceria is reduced. The better performances of the CW-PP catalysts relative to the CW-IMP ones may account for such a behavior.

5. Conclusions

Calcination of the CW-PP catalysts resulted in the formation of a well-dispersed isopolytungstate. However, high W loading led to crystalline $Ce_2(WO_4)_3$ and, probably also, to very small XRD-silent clusters of WO_3. The $Ce_2(WO_4)_3$ should originate from the solid-state reaction between the ceria and the WO_3 phase. For the CW-IMP catalysts, calcination at high temperatures made the presence of WO_3 species clearer. The role of temperature and support is to provide a higher dispersion of these species, which results in a high density of W=O bonds with both an oxidative and a Lewis acid character. These species are able to abstract hydride ions from hexane and to isomerize the resulting carbocation. The formation of alkenes is a key step. The presence of hydrogen in the reaction mixture determines an irreversible transformation of these sites into Brønsted acid sites, these species being able to operate isomerization of the carbocations. But, under a hydrogen atmosphere, the activity of the catalysts decreases due to the reduced capacity of the catalyst to abstract hydride. The role of the support mainly consists of enhancing the oxidative properties of tungsten.

Acknowledgments

We thank the CGRI and the FNRS (National Fund for Scientific Research), Belgium, for financial support.

References

[1] H. Pines, The Chemistry of Catalytic Hydrocarbon Conversion, Academic Press, New York, 1981.
[2] G.A. Olah, J. Lukas, J. Am. Chem. Soc. 90 (1968) 933.
[3] D.G. Barton, S.L. Soled, E. Iglesia, Top. Catal. 6 (1998) 87.
[4] S. Kuba, P.C. Heydorn, R.K. Grasselli, B.C. Gates, M. Che, H. Knözinger, Phys. Chem. Chem. Phys. 3 (2001) 146.
[5] D. Fărcaşiu, F. Ghenciu, J.Q. Li, J. Catal. 158 (1996) 116.
[6] V.C. Holm, G.C. Bailey, US patent 3 032 599, 1962.
[7] M. Hino, K. Arata, J. Chem. Soc. Chem. Commun. 1980 (1980) 851.
[8] V. Adeeva, J.W. de Haan, J. Jänchen, G.D. Lei, V. Schünemann, L.J.M. van de Ven, W.M.H. Sachtler, R.A. van Santen, J. Catal. 151 (1995) 364.
[9] E. Brunner, Catal. Today 38 (1997) 361.
[10] T. Riemer, H. Knözinger, J. Phys. Chem. 100 (1996) 6739.
[11] S. Coman, V. Pârvulescu, P. Grange, V.I. Pârvulescu, Appl. Catal. A 176 (1999) 45.
[12] Z. Hong, K.B. Fogash, R.M. Watwe, B. Kim, B.I. Masqueda-Jimenez, N.-M.A. Santiago, J.M. Hill, J.A. Dumesic, J. Catal. 178 (1998) 489.
[13] C. Morterra, G. Cerrato, F. Pinna, M. Signoretto, G. Strukul, J. Catal. 149 (1994) 181.
[14] V.I. Pârvulescu, S. Coman, V. Pârvulescu, G. Poncelet, Catal. Lett. 52 (1998) 231.
[15] M.G. Falco, S.A. Canavese, R.A. Comelli, N.S. Figoli, Appl. Catal. A 201 (2000) 37.
[16] M. Hino, K. Arata, J. Chem. Soc. Chem. Commun. (1987) 1259.
[17] K. Tanabe, H. Hattori, T. Yamaguchi, Crit. Rev. Surf. Chem. 1 (1990) 1.
[18] E. Iglesia, D.G. Barton, S.L. Soled, S. Miseo, J.E. Baumgartner, W.E. Gates, G.A. Fuentes, G.D. Meitzner, in: Studies in Surface Science and Catalysis, vol. 101, Elsevier Science, Amsterdam, 1996, p. 533.
[19] J.C. Yori, C.R. Vera, J.M. Parera, Appl. Catal. A 163 (1997) 165.
[20] J.G. Santiesteban, J.C. Vartuli, S. Han, R.D. Bastian, C.D.J. Chang, J. Catal. 168 (1997) 431.
[21] M. Scheithauer, T.-K. Cheung, R.E. Jentoft, R.K. Grasselli, B.C. Gates, H. Knözinger, J. Catal. 171 (1997) 191.
[22] M. Hino, K. Arata, Chem. Lett. (1989) 971.
[23] H. Matsuhasi, K. Kato, K. Arata, in: Acid–Base Catalysis II, Kodansha Ltd., Tokyo, 1994, p. 251.
[24] J.R. Shon, H.W. King, J.T. Kin, J. Mol. Catal. 41 (1987) 375.
[25] C.D. Baertsch, S.L. Soled, E. Iglesia, J. Phys. Chem. B 105 (2001) 1320.
[26] S.L. Soled, E. Iglesia, D. Barton, C.D. Baertsch, G. Meitzner, in: International Symposium on Acid–Base Catalysis IV, Book of Abstracts, paper 06, Matsuyama, Japan, 2001.
[27] M. Valigi, D. Gazzoli, I. Pettiti, G. Mattei, S. Colonna, S. De Rossi, G. Ferraris, Appl. Catal. A 231 (2002) 159.
[28] S. Eibl, B.C. Gates, H. Knözinger, Langmuir 17 (2001) 107.
[29] V. Ponec, G.C. Bond, Catalysis by Metals and Alloys, in: Studies in Surface Science and Catalysis, vol. 95, Elsevier Science, Amsterdam, 1995, p. 343.
[30] P. Courty, H. Ajot, C. Marcilly, B. Delmon, Powder Technol. 7 (1973) 21.
[31] M. Yoshimura, F. Sibieude, A. Rouanet, M. Foex, J. Solid State Chem. 16 (1976) 219.
[32] M. Alifanti, C.M. Visinescu, V.I. Pârvulescu, P. Grange, G. Poncelet, in: Studies in Surface Science and Catalysis, vol. 143, Elsevier Science, Amsterdam, 2002, p. 337.
[33] J.F. Moulder, W.F. Sticle, P.E. Sobol, K.D. Bomben, in: J. Chastain (Ed.), Handbook of XPS, Perkin Elmer Corporation, 1992.
[34] E. Paparazzo, G.M. Ingo, N. Zachetti, J. Vac. Sci. Technol. A 9 (1991) 1416.
[35] J.Z. Shyu, J. Catal. 114 (1988) 23.
[36] M. Romeo, Surf. Interface Anal. 20 (1993) 508.
[37] G. Groppi, C. Cristiani, L. Lietti, C. Ramella, M. Valentini, P. Forzatti, Catal. Today 50 (1999) 399.
[38] J.A. Horsley, I.E. Wachs, J.M. Brown, G.H. Via, F.D. Hardcastle, J. Phys. Chem. 91 (1987) 4014.
[39] C. Bigey, L. Hilaire, G. Maire, J. Catal. 198 (2001) 208.
[40] Z. Yu, X. Yang, J.H. Lunsford, M.P. Rosynek, J. Catal. 154 (1995) 163.
[41] L. Blanchard, Ph.D. thesis, Lille, 1984.
[42] V. Cordis, K.-H. Tytko, O. Glemser, Z. Naturforsch. B 30 (1975) 834.
[43] M.A. Centeno, I. Carrizosa, J.A. Odriozola, Appl. Catal. B 29 (2001) 307.
[44] W. Li, J. Hu, Y. Che, Catal. Lett. 53 (1998) 15.
[45] A.J. Bridgeman, G. Cavigliasso, Chem. Phys. 279 (2002) 143.